 ©2019 Kvantovaya Elektronika and Turpion Ltd

https://doi.org/10.1070/QEL17133

A Fabry–Perot interferometer formed in the core of a composite optical fibre heavily doped with phosphorus oxide

O.N. Egorova, S.A. Vasil'ev, I.G. Likhachev, S.E. Sverchkov,
B.I. Galagan, B.I. Denker, S.L. Semjonov, V.I. Pustovoi

Abstract. **We report a new method for manufacturing a Fabry–Perot interferometer in the form of a microcavity in the optical fibre core. The method is based on the use of the process of electric discharge fusion splicing of a conventional optical fibre and a special composite fibre having a core with a high content of phosphorus oxide. The possibility of using this interferometer as a sensitive element of a strain sensor with high temperature stability is shown.**

Keywords: *Fabry–Perot interferometer, strain sensor, composite optical fibre.*

1. Introduction

Among the wide variety of proposed sensors based on Fabry–Perot interferometers (FPIs), designs integrated directly into the optical fibre structure in the form of a cavity are of great interest. Such structures are quite simple, compact, and can be located away from the recording equipment. Currently, there are various methods for the formation of microcavities in the optical fibre core: by micromachining of optical fibre with femtosecond laser pulses [1, 2], through the use of hollow microstructured optical fibres [3–6], by fusion splicing conventional optical fibres [7–9] and fibres with a high content of aluminium oxide in the core [10].

2. Formation of microcavities (FPI)

This paper proposes a new method for the formation of a microcavity in the optical fibre core representing a Fabry–Perot interferometer, and also shows the possibility of using this interferometer as a sensitive element of a strain sensor. The method of FPI formation described in this paper is based on the process of electric discharge fusion splicing of a conventional optical fibre and a special composite fibre with a silica glass cladding and a core with a high content of phosphorus oxide. A special composite fibre was made by sintering of phosphate glass in a silica glass tube (Fig. 1).The material for core fabrication was phosphate glass [11] containing 65 mol% P_2O_5, 7 mol% Al_2O_3, 12 mol% B_2O_3, 9 mol% Li_2O, and 7 mol% Re_2O_3. A hollow cylindrical diamond drill was used to drill out a cylinder in a bulk phosphate glass (Fig. 1a), which was then inserted into a silica glass tube (Fig. 1b). Next,

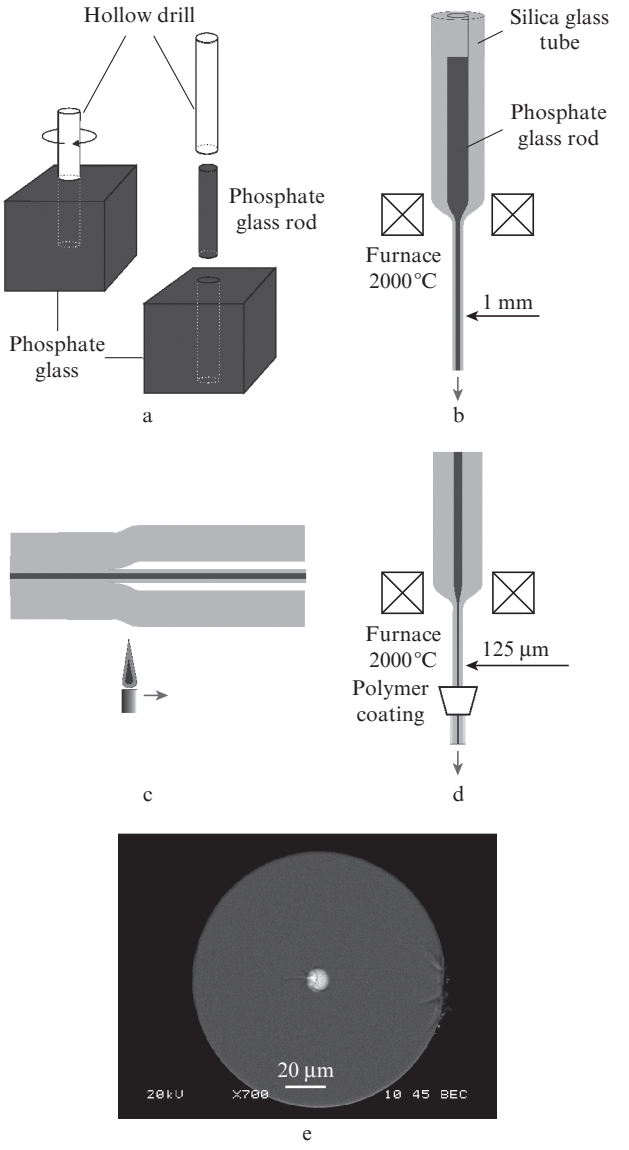

Figure 1. (a–d) Scheme of manufacturing a composite optical fibre and (e) photograph of the end face of the resulting fibre.

O.N. Egorova, I.G. Likhachev, S.E. Sverchkov, B.I. Galagan, B.I. Denker, V.I. Pustovoi Prokhorov General Physics Institute, Russian Academy of Sciences, ul. Vavilova 38, 119333 Moscow, Russia, e-mail: egorova@nsc.gpi.ru;
S.A. Vasil'ev, S.L. Semjonov Fiber Optics Research Center, Russian Academy of Sciences, ul. Vavilova 38, 119333 Moscow, Russia

Received 13 September 2019; revision received 15 October 2019
Kvantovaya Elektronika **49** (12) 1140–1144 (2019)
Translated by M.A. Monastyrskiy

the resulting preform was sintered in the furnace at a temperature of ~2000°C and drawn into rods with a diameter of ~1 mm (Fig. 1b). To ensure the required ratio of the core and clad diameters, the resulting rods, after placing inside an additional silica glass tube, were subjected to jacketing on a glass working lathe equipped with a burner (Fig. 1c). Then, an optical fibre was drawn from the preform obtained (Fig. 1d).

A photograph of the end face of the resulting fibre is shown in Fig. 1e. The fibre core diameter was ~10 μm, and the diameter of the silica glass cladding was 125 μm. In the process of drawing the fibre, of phosphate and silica glasses mutually diffused, leading to a decrease in the concentration of phosphorus oxide in the core glass, amounted to ~35 mol%. The measurements were conducted by X-ray microanalysis using a JSM-5910 LV scanning electron microscope (JEOL) and an INCA X-ray spectrometer (Oxford Instruments). The obtained concentration level was higher than one, which could be obtained using conventional vapour deposition methods. The high concentration of phosphorus oxide caused a significant difference in the physicochemical properties of the core and cladding glasses, in particular, a lower temperature of the formation of volatile components and a higher thermal expansion coefficient (TEC) of the core.

A Fabry–Perot interferometer in the form of a microcavity in the optical fibre core was obtained by electric discharge fusion splicing of a fabricated composite fibre and a conventional SMF-28 telecommunication optical fibre. Figure 2a shows a photograph of microcavity 1 obtained on a Fujikura FSM80 fusion splicer with an arc power of 50 units (only relative values are provided by the fusion splicing machine manufacturer) and a discharge duration of 300 ms (the composite optical fibre is located to the right of the junction point of the optical fibres).

Apparently, the mechanism of the microcavity formation involves the following. At the very beginning of the fusion splicing process, when the electric arc is turned on, the core glass evaporates from the end-face surface of the composite fibre, since it has a lower temperature of the formation of volatile components than the undoped glass of the cladding. As a result, an open cavity is formed on the surface of the fibre end face in the core region. Beyond that, the formation of a cavity on the end-face surface of the fibre in the core region can be stipulated by the relaxation of mechanical strains arising in the process of fibre drawing due to the large difference in the TEC between the core glass and the composite fibre cladding during the heating of the fibre end face at the start of splicing. The resulting open cavity is converted into a microcavity embedded in the fibre core when the end faces of the optical fibres are fusion spliced in the process.

Figures 2b and 2c show photographs of microcavities 2 and 3 obtained by additional heating of the original microcavity 1 by an arc discharge with a duration of 600 and 2300 ms, respectively. It is seen that under the vapour pressure of evaporated glass, the volume of microcavities increases in the longitudinal direction along the low-melting core, and in the case of longer heating, also in the transverse direction due to the expansion of a more refractory silica glass cladding.

3. Study of FPI characteristics. Discussion of results

A scheme for studying the reflection spectra of microcavities (Fabry–Perot interferometers) is shown in Fig. 3. A Super-

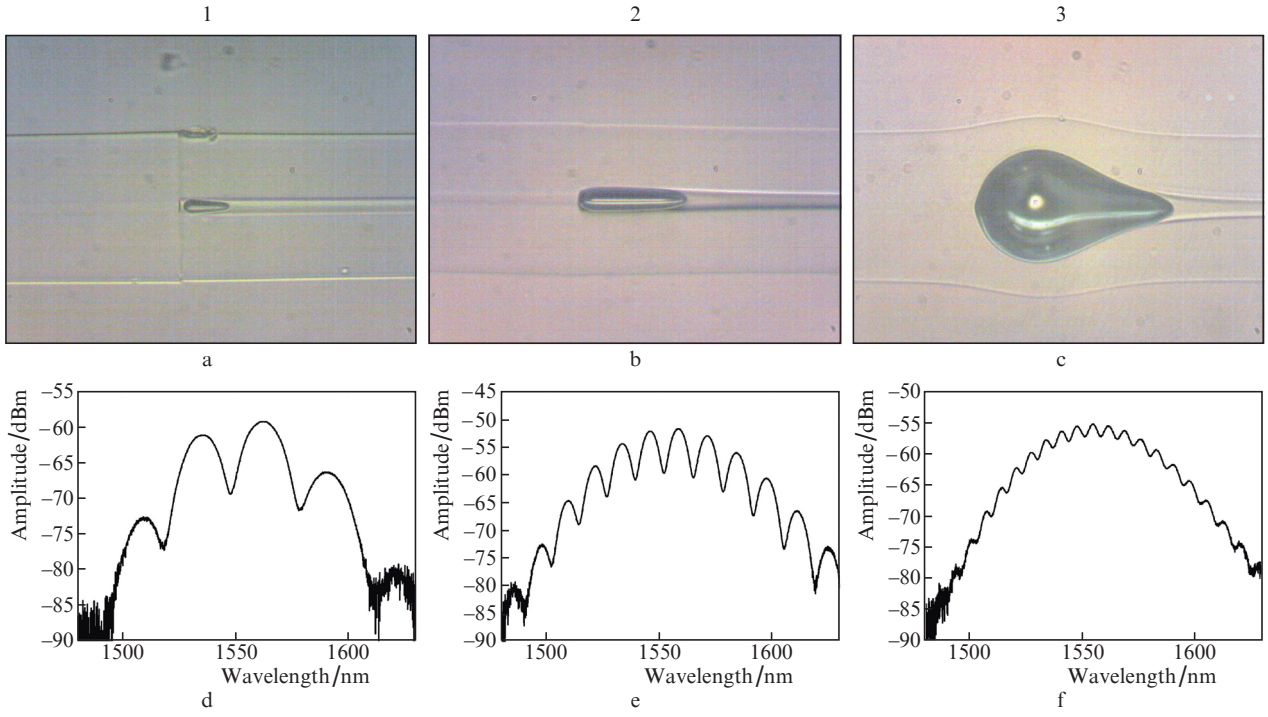

Figure 2. Photographs of microcavities in the fibre core: (a) original cavity at the arc discharge duration of 300 ms and (b,c) cavities from the original cavity after additional heating by the arc discharge of (b) 600 and (c) 2300 ms duration, and also (d–f) reflection spectra of interferometers (d) 1, (e) 2 and (f) 3.

lum SLD-76-MP semiconductor superluminescent diode (SLD) with a spectrum width of 50 nm (at a level of 3 dB) with a centre near $\lambda = 1550$ nm was used as an optical source. The reflected signal was recorded using an ANDO AQ6317B optical spectrum analyser (OSA). The SLD radiation was fed to the input of the fibre-optic circulator, and then passed into a standard single-mode optical fibre, at the junction of which with a composite optical fibre an FPI was located, formed by two gas–glass interfaces, as shown in the inset of Fig. 3. The radiation (signal) reflected from the FPI was supplied to the OSA input by means of a circulator. Figures 2d–2f show the reflection spectra of interferometers 1, 2 and 3.

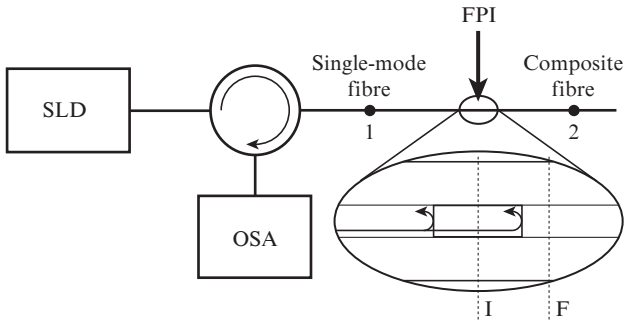

Figure 3. Scheme for recording reflection spectra. The inset shows a schematic representation of the interferometer.

Since the reflection coefficient at the glass–gas interface is small (~4%), the resulting interferometers can be described using a two-beam model. Then, the reflected signal intensity represents an oscillating function with wavelength λ:

$$I = I_1 + I_2 + 2\sqrt{I_1 I_2}\cos\varphi,$$

where I_1 and I_2 are the intensities of the waves reflected from two FPI mirrors (see Fig. 3); $\varphi = 4\pi nL/\lambda$ is the phase difference of these waves; $n \approx 1$ is the refractive index of the gas medium inside the interferometer cavity; and L is the interferometer length. Note that a decrease in the intensity of the reflected signal at the edges of the reflection spectra in Figs 2d–2f is due to the shape of the SLD spectrum. In the process of mathematical processing of the experimental results given below, the reflected signal was normalised to the source spectrum.

The FPI length can be calculated from the difference in wavelengths of adjacent minima (maxima) in the reflection spectrum:

$$L = \lambda_1\lambda_2/2n(\lambda_1 - \lambda_2),$$

where λ_1 and λ_2 are the wavelengths of adjacent minima. The lengths of interferometers 1, 2 and 3, calculated from the period of the reflected signal spectrum (see Figs 2d–2f), constituted 40, 93 and 172 μm, respectively. The modulation amplitude of the reflected signal decreased with increasing interferometer length. This is due to an increase in optical loss caused by the beam divergence in the interferometer when increasing its length [12].

We should note that the process of microcavity formation is well reproducible. Thus, with the same electric arc parameters, the microcavity length variations did not exceed 5%.

The fabricated FPIs were investigated for the effect of temperature and fibre strain on the reflection spectrum. A tensile force to ensure the fibre strain was applied to the fibre section with the interferometer at points 1 and 2 located at a distance of several tens of centimetres from each other (see Fig. 3). For a fibre section with the interferometer having, for example, a cylindrical surface of the side walls, as shown in the inset in Fig. 3, the applied force F, in accordance with Hooke's law, determines, firstly, the relative elongation of the interferometer $\Delta L_I/L_I = F/(ES_I)$ (S_I is the cross-sectional area of the side walls of the silica glass interferometer in plane I, E is Young's modulus of silica glass, L_I is the interferometer length, and ΔL_I is the increase in interferometer length), and secondly, the relative elongation $\Delta L_F/L_F = F/(ES_F)$ of the optical fibre outside the interferometer (S_F is the cross-sectional area of the optical fibre in plane F, L_F is the fibre length between points 1 and 2 minus the interferometer length, and ΔL_F is the increase in the fibre length within this section). It is assumed that Young's modulus is the same for the core glasses and fibre cladding. Since $L_I \ll L_F$, and S_F and S_I are comparable in magnitude, the relative elongation of the entire fibre section between points 1 and 2 is

$$\frac{\Delta L_{12}}{L_{12}} = \frac{\Delta L_I + \Delta L_F}{L_{12}} = \frac{F}{EL_{12}}\left(\frac{L_I}{S_I} + \frac{L_F}{S_F}\right) \approx \frac{\Delta L_F}{L_F},$$

and consequently,

$$\frac{\Delta L_I}{L_I} = \frac{\Delta L_{12}}{L_{12}}\frac{S_F}{S_I}.$$

Thus, the relative elongation of the FPI is linearly related to the applied force F (or relative elongation of the entire optical fibre between points 1 and 2).

Using the minimum condition in the interferometer reflection spectrum $\varphi = 4\pi nL_I/\lambda = \pi(2m + 1)$, where m is an integer, we arrive at the following relation for the shift $\Delta\lambda$ of the minimum position as a result of a change in the FPI length:

$$\frac{\Delta\lambda}{\lambda} = \frac{\Delta L_I}{L_I}. \qquad (1)$$

Thus, the ratio $\Delta\lambda/\lambda$ linearly depends on the relative elongation of the interferometer, which in turn is linearly related to the applied force F and the relative elongation of the fibre itself (fibre strain).

Figure 4a shows the reflection spectra of interferometer 1 with $\Delta L_{12}/L_{12}$ increasing from 0 to 2160 μm m^{-1}. The dependences of the wavelength shifts $\Delta\lambda$ of the signal minimum in the vicinity of $\lambda = 1550$ nm in the reflection spectra of interferometers 1, 2 and 3 on the fibre strain, as well as on the applied mechanical load are shown in Fig. 4b. The sensitivity to mechanical deformation of FPIs 1 and 2 is ~1.7 pm μm^{-1} m, and FPI 3 – 2.3 pm μm^{-1} m (in the English literature, μm m^{-1} corresponds to the measurement unit of fibre strain $\mu\varepsilon$). The sensitivity value obtained is comparable, for example, with the results of work [3, 4]. Note that for fibre Bragg gratings, which are in active use as sensitive elements of strain sensors, this value for $\lambda \approx 1.55$ μm is ~1.1 pm μm^{-1} m [13].

When applying a longitudinal mechanical load, the sensitivity of FPI 3 slightly exceeds that of FPI 1 and FPI 2. As seen from Fig. 2, the cross-sectional diameter of microcavity 3 exceeds that of cavities 1 and 2, while, in the longitudinal section, microcavity 3 has the characteristic shape

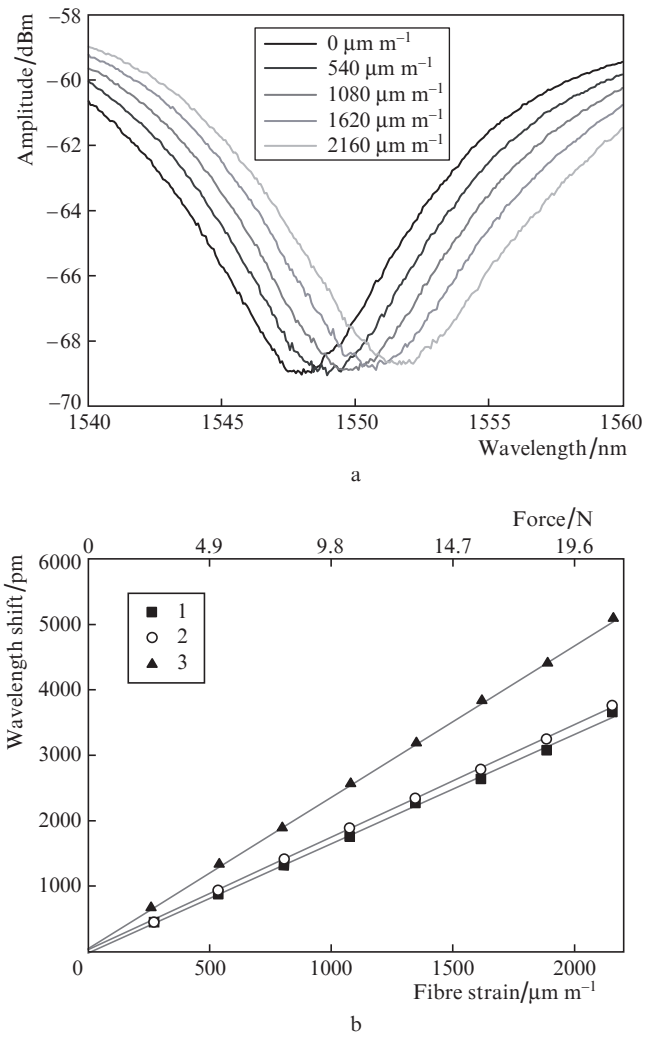

Figure 4. (a) Reflection spectra of FPI 1 at various fibre strains $\Delta L_{12}/L_{12}$ and (b) wavelength shifts $\Delta\lambda$ of one of the minima (near λ = 1550 nm) in the reflection spectra of FPI 1, 2 and 3 vs. the fibre strain $\Delta L_{12}/L_{12}$ and applied force F.

of an inflated bubble with curvilinear boundaries of the side walls. In accordance with Hooke's law, a decrease in the cross-sectional area of the side walls could lead to an increase in elongation. However, the image analysis shown in Figs 2a–2c does not indicate such a decrease. An additional increase in the sensitivity of microcavity 3 is most likely associated with a change in the cross-sectional shape of the microcavity in the longitudinal direction under tensile forces.

To study the temperature sensitivity of interferometers, they were placed in a tubular furnace and heated from room temperature of 25 °C to a temperature of 500 °C with a step of 50 °C. The experimental data obtained for the minima in the reflection spectra closest to λ = 1550 nm, and also the results of their approximation by a linear dependence are presented in Fig. 5. Note that the temperature sensitivity $\Delta\lambda/\Delta T$ of the studied samples is quite small and only amounts to 1.1 pm °C^{-1} for FPI 1 and FPI 3, and 0.9 pm °C^{-1} for FPI 2. The data obtained are in good agreement with the results of work [3–8]. The value $\Delta\lambda/(\lambda\Delta T) = \Delta L_I/(L_I\Delta T)$ [see (1)] for a wavelength of 1550 nm at which the measurements were performed constituted about 6.5×10^{-7} °C^{-1}, which was close to the TEC value for silica glass, which, according to work [14], amounted to $(4.17–5.92) \times 10^{-7}$ °C^{-1} in the temperature range of 50–500 °C. Therefore, the temperature sensitivity of the manufactured interferometers is mainly determined by the TEC of the side walls of the microcavities made of undoped silica glass. Such low FPI temperature sensitivity, due to the small TEC of silica glass, distinguishes it favourably from fibre Bragg gratings, in which this value is an order of magnitude greater [13], and allows for some tasks not to resort to additional temperature compensation of the sensor readings.

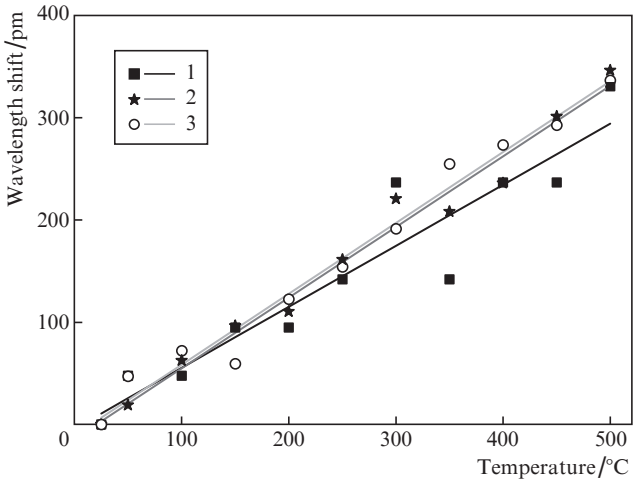

Figure 5. Temperature dependences of the minimum wavelength in the vicinity of λ = 1550 nm in the reflection spectra of interferometers 1, 2 and 3 heated from room temperature to 500 °C.

Heating of the FPI to a temperature of 500–600 °C was reversible, i.e., when the temperature decreased after heating, the positions of the minima and maxima in the reflection spectrum returned to the values corresponding to the initial temperature. However, when heated to a temperature of 700 °C, an irreversible increase in the interferometer length was observed. This irreversible change can be used to accurately select the interferometer operating point in the case of narrowband radiation.

Thus, we have proposed a new method for designing a Fabry–Perot interferometer integrated directly into the optical fibre structure. The method is based on the electric discharge fusion splicing of a single-mode fibre based on silica glass and a composite fibre obtained by sintering phosphate glass in a silica glass tube. The possibility of using the developed interferometer as a sensitive element of the strain sensor is shown. Low temperature sensitivity in comparison with fibre Bragg gratings makes the described type of sensing elements of a strain sensor promising for practical applications.

References

1. Rao Y.J., Deng M., Duan D.W., Yang X.C., Zhu T., Cheng G.H. *Opt. Express*, **15**, 14123 (2007).
2. Wei T., Han Y.K., Tsai H.L., Xiao H. *Opt. Lett.*, **33**, 536 (2008).
3. Li E., Peng G.-D., Ding X. *Appl. Phys. Lett.*, **92**, 101117 (2008).
4. Villatoro J., Finazzi V., Coviello G., Pruneri V. *Opt. Lett.*, **34**, 2441 (2009).
5. Ferreira M.S., Bierlich J., Kobelke J., Schuster K., Santos J.L., Frazão O. *Opt. Express*, **20**, 21946 (2012).

6. Favero F.C., Araujo L., Bouwmans G., Finazzi V., Villatoro J., Pruneri V. *Opt. Express*, **20**, 7112 (2012).
7. Liu S., Wang Y., Liao C., Wang G., Li Z., Wang Q., Zhou J., Yang K., Zhong X., Zhao J., Tang J. *Opt. Lett.*, **39**, 2121 (2014).
8. Duan D.W., Rao Y., Hou Y.-S., Zhu T. *Appl. Opt.*, **51**, 1033 (2012).
9. Machavaram V.R., Badcock R.A., Fernando G.F. *Sensors and Actuators A*, **138**, 248 (2007).
10. Ma Z., Pang F., Liu H., Chen Z., Wang T. *Proc. Conf. on Optical Fiber Sensors* (Lausanne, 2018) WF48.
11. Karlsson G., Laurell F., Tellefsen J., Denker B., Galagan B., Osiko V., Sverchkov S. *Appl. Phys. B*, **75**, 41 (2002).
12. Cibula E., Donlagic D. *Opt. Express*, **15**, 8719 (2007).
13. Kersey A.D., Davis M.A., Patrick H.J., LeBlanc M., Koo K.P., Askins C.G., Friebele E.J. *IEEE J. Lightwave Technol.*, **15**, 1442 (1997).
14. Leko V.K., Mazurin O.V. *Svoistva kvartsevogo stekla* (Silica Glass Properties) (St. Petersburg: 'Nauka', 1985) p. 166.